Smooth multi-sided blending of biquadratic splines

Kęstutis Karčiauskas[a], Jörg Peters[b]

[a] *Vilnius University*
[b] *University of Florida*

Abstract

Biquadratic (bi-2) splines are the simplest choice for converting a regular quad meshes into smooth tensor-product spline surfaces. Existing methods for blending three, five or more such bi-2 spline surfaces using surface caps consisting of pieces of low polynomial degree suffer from artifacts ranging from flatness to oscillations. The new construction, based on reparameterization of the bi-2 spline data, yields well-distributed highlight lines for a range of challenging test data. The construction uses n pieces of degree bi-4 (bi-3 when $n \in \{3, 5\}$) and applies both to primal (Catmull-Clark-like) and dual (Doo-Sabin-like) input layouts.

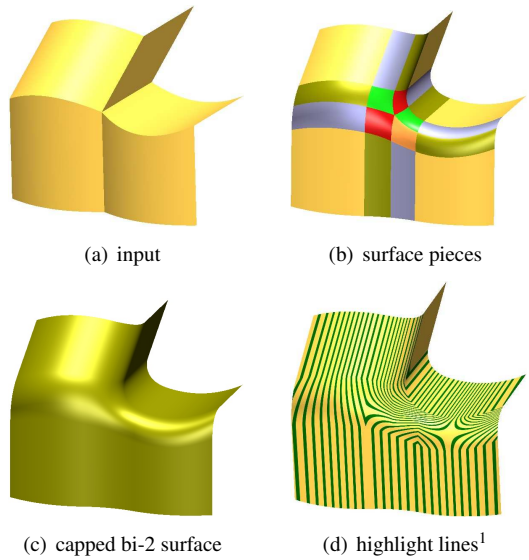

(a) input (b) surface pieces

(c) capped bi-2 surface (d) highlight lines[1]

Figure 1: Pairwise joining and **capping a collection of bi-2 spline surfaces**. (a) Input: one planar and four cylindric pieces. (b) The input is pairwise blended by bi-2 splines and the remaining gap is filled by a G^1 cap consisting of five patches of degree bi-3. (c) output and (d) surface interrogation.

1. Introduction

Many mechanical parts and inner surfaces require only first order smoothness, i.e. continuity of the normal. The simplest tensor-product patch type to match the requirements is the bi-quadratic (bi-2) spline patch. Keeping the degree lower than bi-3 for the bulk of the surface simplifies downstream use, say for iso-geometric computations, and reduces the chance of introducing unwanted visible ripples and oscillations[1].

A classical challenge, illustrated in Fig. 1, is to smoothly blend, by a surface 'cap', three, five or more bi-2 spline patches. Numerous publications in the late 1980s and early 1990s (see the literature survey in Section 2 below) addressed the algebraic constraints for smoothness, but did not focus on shape. To illustrate this claim, we analyze the canonical representatives of the two main alternatives for such blends: subdivision algorithms and Bézier patch constructions. The shape of surfaces generated by the subdivision naturally associated with bi-2 surfaces, the Doo-Sabin algorithm [2], suffers from oscillations near and flatness at the center of the cap (Fig. 2b). Similarly, older (1990s-style) multi-patch Bézier caps of low degree, such as the bi-3 construction of [3] in Fig. 2e, result in poorly-spaced and poorly shaped highlight lines. While our surfaces will not be curvature continuous throughout, as are recent more costly constructions such as [4, 5], they are of low polynomial degree, show remarkably good highlight line distribution for a gallery of challenging test data, and use fewer patches than other low-degree CAD-compatible constructions (cf. [6, 7]).

Contribution. The focus and contribution of this paper is a simple, yet subtle recipe for constructing *low-degree multi-sided surface caps* that complete a bi-2

[1] In surface interrogation, highlight lines are a commonly-used approximation to a parallel arrangement of tube lights in a car show room [1]

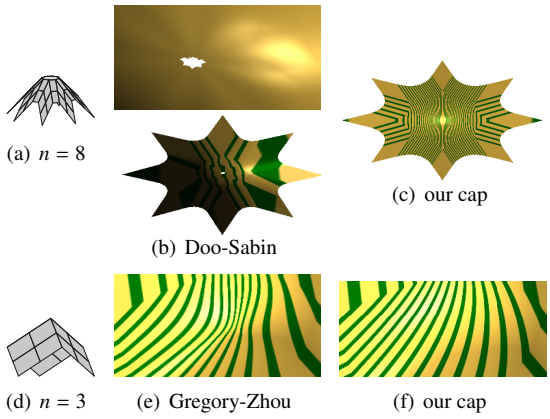

Figure 2: **Artifacts of low-degree caps** for biquadratic splines. (a) Convex input suitable for Doo-Sabin surfaces. (b) Oscillation (and flatness) of Doo-Sabin subdivision surfaces near the central point; compare with our construction (c). For input (d), [3] yields (e) a pinched surface near the central point. Compare with our construction (f).

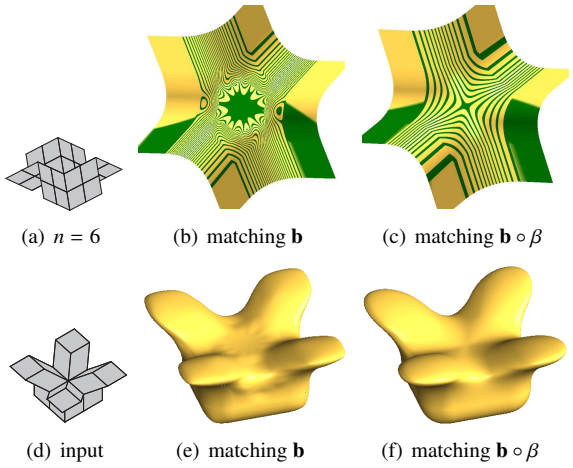

Figure 3: **Importance of reparameterizing the Hermite boundary data.** (a,d) input meshes. The surfaces in (b) and (c) have the same structure and number of bi-3 patches; as do those in (e) and (f). (b,e) show a classical construction (here [3]) extending the data $\mathbf{b}$ without reparameterization. (b) shows a flat center region, (e) shows oscillations. (c,f) our bi-3 construction that extends $\mathbf{b} \circ \beta$, i.e. $\mathbf{b}$ reparameterized by β.

C^1 spline complex and do not suffer from the highlight line artifacts of existing methods. The construction applies both to primal (Catmull-Clark-type) and dual (Doo-Sabin-type) input layouts, i.e. to quad meshes including nodes that have $n \neq 4$ neighbors and to faces with $n \neq 4$ edges.

The construction is a recipe in that it expresses all BB- (Bernstein-Bézier) coefficients of the cap directly in terms of the input mesh. No equations have to be solved at runtime: the final surface is a linear combination of precomputed generating functions.

The construction is subtle and different from older constructions in that it (i) leverages carefully chosen *reparameterizations* β (a bi-variate change of variables) of the Hermite data $\mathbf{b}$ (position and derivative) provided to the cap by the bi-2 splines surrounding the cap and (ii) enforces curvature continuity at the central point. As illustrated in Fig. 3 and explained in more detail in Section 4.1, reparameterizing $\mathbf{b}$ yields better results, visible even without highlight lines. Compare Fig. 3e to Fig. 3f.

Overview. Section 2 reviews the literature and motivates the features of the new algorithm. Section 3 formally introduces the problem to be solved: smoothly filling a multi-sided hole in a bi-2 spline complex. Section 4 introduces the n-sided cap. By default, the cap consists of n patches of degree bi-4, one per sector; when $n \in \{3, 5\}$, well-shaped caps of degree bi-3 per sector can be substituted (Section 4.2). (Appendix C demonstrates that if we split each sector, into 2×2 pieces, degree bi-3 work also for $n > 5$, albeit at the cost of slightly lower quality than the main bi-4 construction of Section 4.) Section 5 demonstrates the quality of the new G^1 caps when completing bi-2 spline models.

2. Background and motivation

Developed in the late 1980s and early 1990s, the theory of geometric continuity (G^1 continuity [8, 9]) provides a foundation for solving the problem of completing a spline surface with tangent plane continuity where n surface pieces meet. The theory spawned a number of innovative algorithms: cap constructions with built-in singularities [10, 11]; normalized by averaging, hence rational surface extensions [12]; restrictions of higher-variable constructions [13]; splitting of the domain into three-sided patches [14, 15, 16] and global manifold constructions [17, 18] employing variants of simplex splines [19], to name just a few. Each class of methods has to overcome the challenge that an object of genus other than one, i.e. topologically different from the torus, does not admit a globally regular, shift-invariant tiling but must have one or more extraordinary points (topological singularities). In fact, when the surface pieces are twice continuously differentiable, all constructions have to solve a vertex-enclosure problem, see e.g. [9]: at even-valence vertices, a matrix of smoothness constraints (in terms of the mixed derivatives that one would naturally associate with the solution) is not invertible.

With the exception of Gregory's singular construction [11], none of these innovative solutions are known to have been adopted by industry. There are multiple reasons for this. First, the methods listed are not compatible with the CAD-industry's NURBS standard. Second, most CAD packages follow a different paradigm to fill multi-sided holes. Solidworks, for example, fits the graph of a function to the data along a boundary and trims off extraneous parts of the resulting many-knot spline surface. The output surfaces may not be watertight and require 'healing' before FEM analysis can be applied. The entertainment industry, led by Pixar, has adopted Catmull-Clark subdivision as a modeling tool. Subdivision surfaces are conceptually simple in that they evoke mesh refinement. Catmull-Clark (CC) [20] subdivision provides sufficient quality for animation but has not entered main stream CAD processing both because it only generalizes uniform polynomial splines and because the resulting surfaces consist of infinitely many pieces. Moreover, the quality of CC subdivision surfaces near the limit point is insufficient [21] (see also Fig. 10a). Doo-Sabin subdivision has had little exposure since it is a 'dual' subdivision method, i.e. shifts the faceted approximation under refinement. The severe artifacts of Doo-Sabin subdivision (e.g. Fig. 2b) do not seem to have been documented before.

There is a growing class of hole-filling constructions that are compatible with tensor-product splines. While constructions of least degree, bi-2 [22], can not correctly handle higher-order saddles, but generate flat spots, the 1990s constructions of degree bi-3, e.g. [23, 3], formally satisfy the smoothness constraints. However, as illustrated in Fig. 2 and Fig. 3, the shape of the surfaces generated by these approaches often disappoints. The current paper shines some light on the causes by emphasising the need for boundary data reparameterization.

To improve shape, functionals of the type

$$\mathcal{F}_m f := \int_0^1 \int_0^1 \sum_{i+j=m, i,j\geq 0} \frac{m!}{i!\,j!} (\partial_s^i f \partial_t^j f)^2,$$

$$\mathcal{F}_\kappa^* f := \int_0^1 \int_0^1 (\partial_s^\kappa f)^2 + (\partial_t^\kappa f)^2,$$

acting on each coordinate of a surface independently, have been advocated as 'fairness functionals' or 'energy minimization' [24, 25, 26, 27, 28, 29]. If the first fundamental form of the resulting surfaces is close to the identity, e.g. if the parameterization in uniform, these functionals can be viewed as penalizing deviation from a surface of low polynomial degree and this may prevent high oscillations. Indeed, [4] uses $\mathcal{F}_4^*$ to set extraneous degrees of freedom when capping a bi-3 spline complex by a cap of degree bi-7 and the resulting surfaces are generally very good. If the justification for using $\mathcal{F}_k^*$ has general merit, $\mathcal{F}_3^*$ should be used for capping bi-2 splines. However, our experiments, some of which are shown in this paper, amply illustrate that functionals fail to produce desirable highlight lines *unless the parameterization is carefully adjusted beforehand*. Here 'desirable highlight lines' means, that, for a number of hard test cases and valences from 3 to 10, the highlight lines are as uniformly distributed as the data permit, avoiding sharp corners or kinks and not bunching up unnecessarily (cf. Fig. 2e vs. Fig. 2f, Fig. 3b vs. Fig. 3c and Fig. 3e vs. Fig. 3f).

Given that a prudent choice of parameterization is an important pre-condition for successfully using functionals $\mathcal{F}_k$ or $\mathcal{F}_k^*$, we observed that the older low-degree algorithms that exhibit poor highlight line distributions all extend the C^1 boundary data without reparameterization. (The algorithm in [30] does reparameterize the boundary, but the surfaces consist of triangular patches of such low degree that they fail to provide the quality we seek.) At first glance a C^1 extension of the boundary data looks natural. But the central point of an n-sided piecewise polynomial cap typically has a parameterization far from uniform; and the transition from the tensor-product to the arrangement of the parameter lines at the center of the surface cap seems to require more degrees of freedom and space than these low-degree C^1 extension algorithms can allocate. By contrast, our construction reparameterizes the boundary data to speed up transition and achieve a more uniform change in the parameterization. Only then do we apply functionals in the controlled setting of determining a few free parameters at a time to finally condense the best choices into simple formulas.

3. Problem Statement: Multi-sided holes in a bi-2 spline complex

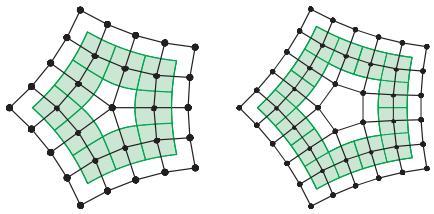

(a) CC-net (primal) (b) DS-net (dual)

Figure 4: **Basic input configurations**: (CC-net) all faces are quads, but nodes need not be 4-valent; (DS-net) all nodes are 4-valent, but faces can be multi-sided.

Fig. 4 shows two multi-sided hole configurations for a quad-mesh that can be interpreted as control points of a bi-2 spline surface: the CC-net, where all faces are quads, but nodes need be not 4-valent, and the DS-net, where all nodes are 4-valent, but faces can be multi-sided. The green ring of bi-2 patches provides the context since the transition from the spline complex into the cap is as important as the quality of the cap itself. The cap construction will only use the central point and the first layer of points surrounding it. Therefore non-4-valent points in CC-nets may be adjacent.

Applying the bi-2 tensor-product spline refinement rules (see Fig. 5) transforms a CC-net into a DS-net and unifies the treatment of both configurations to that of Fig. 6b. Applied globally, such refinement quadruples the number of pieces. So this is not done here: the input is not subdivided. Rather, a virtual refinement step is applied within the algorithm as illustrated in Fig. 6.

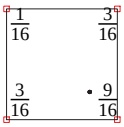

Figure 5: **Bi-2 stencil**.

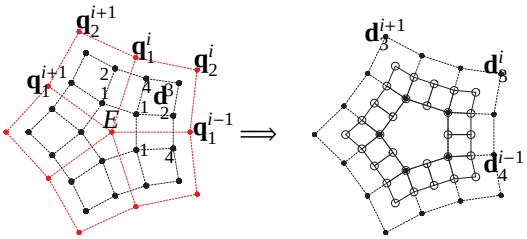

(a) virtual refinement (b) tensor-border **b**

Figure 6: **Unification of input CC-net and input tensor-border.** (a) A local, virtual refinement step unifies the input configurations of Fig. 4. In the main text, only the DS-net points $\mathbf{d}^i_j$, $j \in \{1,2,3,4\}$ (black disks) are used. Appendix A specifies a construction in terms of primal input points $\mathbf{q}^i_j$. (b) The solid-line tensor-border **b** (= ring of position and derivative data in BB-form) is the unified input to the algorithm.

We can therefore specify the algorithm as constructing a cap to match the *tensor-border* **b** of a surface ring of degree bi-2 (green in Fig. 4b). The tensor-border represents the position and transversal derivative of its inner boundary in terms of the BB-net (Bernstein-Bézier net) as illustrated in Fig. 6b. This point of view allows arbitrary net layouts as long as extraordinary facets, Fig. 4b, do not share a vertex and their edges have no extraordinary nodes. Extraordinary nodes, Fig. 4a, need not be separated.

Gallery of CC-nets. Defining good shape is hard. One school of thought is that oscillations (not already present in the tensor-border data) are to be avoided. While oscillations on the final surface can be visualized, for example via highlight lines, a practical mathematical characterization to prevent unwanted oscillations has remained illusive. Many examples in the present paper illustrate that one cannot hope to get good results simply by minimizing an energy measure over all free parameters. We therefore apply the construction to a gallery of carefully selected, structurally simple test input nets, for valences up to 10. Fig. 7 shows some of these. We found and illustrate in Section 5 that our parameters optimized with respect to the gallery work well also in more general scenarios. Parts of our test nets are intentionally planar in order to generate easily understood, zero curvature parts of the tensor-border. (If the tensor-border is itself complex, it is difficult to predict the expected or desirable highlight line distribution of the surface cap.) Convex CC-nets, such as Fig. 7e are especially sensitive to functionals and to the choice of central point position.

(a) $n = 5$ (b) $n = 6$ (c) $n = 7$ (d) $n = 8$ (e) $n = 10$

Figure 7: Some **extended CC-nets**: (a) off-center peak, (b) beams joining, (c) higher-order saddle, (d) 'house' corner, (e) convex hat.

4. Construction: Multi-sided caps of *n* patches completing a bi-2 spline complex

By default, our n-sided cap consists of n tensor-product patches of degree bi-4. That is, they can be represented as maps $\mathbf{p} : (u,v) \to \sum_{i=0}^{4}\sum_{j=0}^{4} \mathbf{p}_{ij} B_i^4(u) B_j^4(v) \in \mathbb{R}^3$, where $B_\ell^d(t) := \binom{d}{\ell}(1-t)^{d-\ell}t^\ell$ is the ℓth Bernstein-Bézier (BB-) polynomial of degree d and $\mathbf{p}_{ij}$ are the BB-coefficients. (Section 4.2 additionally exhibits well-shaped caps of degree bi-3 that can be used where $n \in \{3,5\}$.) These n patches, one per sector, share and surround a central point. A key innovation of the construction over older ones is the interplay between the reparameterizations ρ between pieces of the cap, β along the cap boundary and σ to determine the curvature-continuous center.

G¹ *continuity between sectors.* Adjacent patches (see Fig. 8) $\grave{\mathbf{p}} := \mathbf{p}^k$ and $\acute{\mathbf{p}} := \mathbf{p}^{k+1}$, $k = 0,\dots,n-1$ (superscript modulo n) join along their shared boundary curve $\grave{\mathbf{p}}(u,0) = \acute{\mathbf{p}}(u,0)$ with G^1 continuity, i.e. C^1 continuity

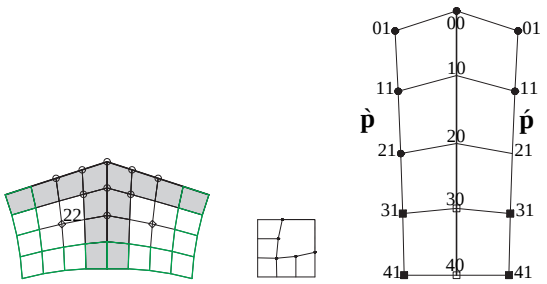

(a) bi-4 layout (b) β (c) G^1 strip

Figure 8: **Bi-4 cap construction.** (a) Adjacent bi-4 patches of the cap (green parts of the BB-net are determined by $\mathbf{b}\circ\beta$). (b) The reparameterization β of the tensor-border $\mathbf{b}$. (c) Labels along the G^1 strip, grey in (a), of BB-coefficients $\grave{\mathbf{p}}_{ij}$, $\acute{\mathbf{p}}_{ij}$, $i = 0..4$, $j = 0, 1$ relevant for the G^1 join between adjacent patches: black disks mark BB-coefficients still free to choose after resolving the G^1 constraints by assignment (2).

after a change of variables. Specifically, with the subscript v indicating the partial derivative in the direction transversal to the sector boundary and u along the sector boundary,

$$\acute{\mathbf{p}}_v + \grave{\mathbf{p}}_v = 2\mathsf{c}(1-u)\grave{\mathbf{p}}_u, \quad \text{where } \mathsf{c} := \cos\frac{2\pi}{n}. \tag{1}$$

In terms of the BB-coefficients (see Fig. 8c for subscripts), it is easily checked that G^1 continuity follows from setting

$$\begin{aligned}
\grave{\mathbf{p}}_{10} &:= \frac{2(\mathsf{c}-1)\grave{\mathbf{p}}_{00} + \grave{\mathbf{p}}_{01} + \acute{\mathbf{p}}_{01}}{2\mathsf{c}};\\
\grave{\mathbf{p}}_{20} &:= \frac{4\mathsf{c}(\grave{\mathbf{p}}_{11} + \acute{\mathbf{p}}_{11}) + (3\mathsf{c}-4)(\grave{\mathbf{p}}_{01} + \acute{\mathbf{p}}_{01} + 2(\mathsf{c}-1)\grave{\mathbf{p}}_{00})}{6\mathsf{c}^2};\\
\acute{\mathbf{p}}_{21} &:= -\grave{\mathbf{p}}_{21} + 2\grave{\mathbf{p}}_{20} + \mathsf{c}(\grave{\mathbf{p}}_{30} - \grave{\mathbf{p}}_{20});\\
\grave{\mathbf{p}}_{30} &:= \frac{4(\grave{\mathbf{p}}_{31} + \acute{\mathbf{p}}_{31}) - \mathsf{c}(\grave{\mathbf{p}}_{41} + \acute{\mathbf{p}}_{41})}{2(4-\mathsf{c})};\\
\grave{\mathbf{p}}_{40} &:= \frac{\grave{\mathbf{p}}_{41} + \acute{\mathbf{p}}_{41}}{2}.
\end{aligned} \tag{2}$$

G^1 *join of cap and surrounding data.* A key choice of the construction is the formula for $\grave{\mathbf{p}}_{30}$. The BB-coefficient $\grave{\mathbf{p}}_{30}$ is compatible with the C^1 tensor-border data $\mathbf{b}$ only after change of variables: the cap joins C^1 with $\mathbf{b}\circ\beta$ for a suitable change of variables β. The Taylor expansion of β with respect to v along an edge of $\mathbf{p}^k$ parameterized by u is $(u + b(u)v, a(u)v)$, where

$$\begin{aligned}
&b(u) := \sum_{i=0}^{3} b_i B_i^3(u),\ a(u) := \sum_{i=0}^{2} a_i B_i^2(u);\\
&a_0 := 1, \quad a_1 := \frac{2-c}{2}a_2, \quad a_2^{def} := \frac{n-2}{0.55n-0.2},\\
&b_0 := 0,\ b_1 := -\frac{2}{3} + \frac{2-c}{3}a_2,\ b_2^{def} := 0,\ b_3 := 0.
\end{aligned} \tag{3}$$

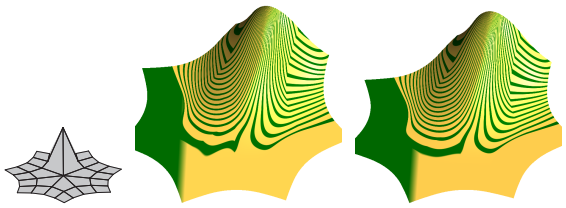

(a) input (b) without setting $\mathbf{p}_{22}$ (c) our cap

Figure 9: Improving highlight line distribution by (c) **setting $\mathbf{p}_{22}$ according to** (4) rather than (b) computing it by minimization.

Here and later, the superscript ^{def} identifies values unrestricted by smoothness (compatibility) constraints and set by considerations discussed in detail in Appendix B. The reparameterization β preserves the boundary of the bi-2 spline complex and is symmetric with respect to the diagonal $u = v$, see Fig. 8b.

Completing the bi-4 cap. Fig. 8a shows the structure of the bi-4 patches. The green control subnet is defined by $\mathbf{b}\circ\beta$, the gray regions satisfy the G^1 constraints (2), the circles near the center are coefficients that define a quadratic expansion at central point. (A second important feature of the construction is that the patches meet G^2 at the central point.) The coefficients $\mathbf{p}_{22}$ are set to the symmetric average

$$\begin{aligned}
\mathbf{p}_{22} := &\frac{1}{2}\Big(\frac{2}{3}(\mathbf{p}_{12} + \mathbf{p}_{32}) - \frac{1}{6}(\mathbf{p}_{02} + \mathbf{p}_{42})\Big)\\
&+ \frac{1}{2}\Big(\frac{2}{3}(\mathbf{p}_{21} + \mathbf{p}_{23}) - \frac{1}{6}(\mathbf{p}_{20} + \mathbf{p}_{24})\Big).
\end{aligned} \tag{4}$$

(The pattern $\frac{2}{3}(\mathbf{p}_1 + \mathbf{p}_3) - \frac{1}{6}(\mathbf{p}_0 + \mathbf{p}_4)$ indicates that the degree of the associated curve is reduced to 3.) Fig. 9 shows the beneficial effect on the shape when setting $\mathbf{p}_{22}$ according to (4) rather than as part of globally minimizing a functional.

The central point is defined as the average

$$eop := ne\sum_{k=0}^{n-1}\frac{\mathbf{d}_1^k}{n} + (1-ne)\sum_{k=0}^{n-1}\frac{\mathbf{d}_2^k + \mathbf{d}_4^k}{2n}, \tag{5}$$

of the input point $\mathbf{d}_j^k$ (Fig. 6b). The default weight e is calibrated by experiment, on a large set of inputs including Fig. 7, to be

$$e^{def} := \frac{1.5+\epsilon}{n+1.6}, \quad \epsilon := \begin{cases} 0 & \text{for } n \in \{5,6,7\};\\ n/100 & \text{for } n \in \{8,9,10\}. \end{cases}$$

This leaves undetermined n+5 BB-coefficients: the five remaining coefficients of the quadratic expansion at the center and the n coefficients $\mathbf{p}_{21}^k$ (see $\grave{\mathbf{p}}_{21}$ in Fig. 8c). For

reasons laid out in Section 4.1, these $n+5$ degrees of freedom are chosen to minimize, over all n bi-4 patches $\mathbf{p}^k$, the functional $\mathcal{F}_3(\mathbf{p})$ when $n \in \{5,6,7\}$ and the functional $\mathcal{F}_4(\mathbf{p})$ when $n \in \{8,9,10\}$.

Implementation. The resulting linear system of size $(n+5)\times(n+5)$ is the same in each coordinate and does not depend on data other than the valence n. Therefore, we can pre-compute its solution for fixed n. Specifically, we tabulate the *four generating functions* corresponding to the points $\mathbf{d}^k_m$, $m = 1,2,3,4$, of the DS-net Fig. 6b. That is, we set $\mathbf{d}^0_m = 1$ for one of $m = 1,\ldots,4$ and all other $\mathbf{d}^k_m = 0$ and compute the coordinate-wise (scalar-valued) bi-4 coefficients

$$h^{k,m}_{ij},\ k = 0,\ldots,n-1,\ m = 1,\ldots,4,\ i,j \in \{0,\ldots,4\}$$

according to the algorithm. These $h^{k,m}_{ij}$ have been tabulated for easy implementation. Then the geometric control points of the patch covering sector s are

$$\mathbf{p}^s_{ij} := \sum_{k=0}^{n-1}\sum_{m=1}^{4} h^{k,m}_{ij}\mathbf{d}^{s-k}_m. \tag{6}$$

If the input is a CC-net then we can express the solution even more succinctly, in terms of only the vertices of the quads surrounding the central point (see Appendix A). This has the welcome effect of reducing the work since there are only $2n+1$ CC-net points compared to $4n$ DS-net points. The formulas of Appendix A subsume the virtual subdivision step explained in Section 3.

4.1. Construction decisions

Some careful choices of parameterization are reflected in the construction. To consistently obtain a good distribution of control points and ultimately of the highlight lines, it is critical to judiciously set parameters of the reparameterization β across the boundary (recall Fig. 3) and the reparameterization σ at the center. Our choices are based on extensive testing against challenging input data and on considerations of symmetry and uniformity.

Reparameterizing the tensor-border with β. Fig. 3 already indicated that a bi-3 construction (even though using 2×2 patches per sector of the cap) results in poor shape when interpolating the tensor-border $\mathbf{b}$ directly without reparameterization. As illustrated in Fig. 10b,e, constructions of degree bi-4 [29] fare no better when they so extend the bi-2 splines. The reparameterization β is carefully crafted to interact with the reparameterization ρ between the sectors – to enable the solution (2), see Fig. 10. Our specific choice of a_2^{def} is motivated by symmetry and b_2^{def} (stretching the tangent data) by the uniform distribution of control points as exemplified in the reparameterization σ of Appendix B. The positive effect of using β is demonstrated in Fig. 10.

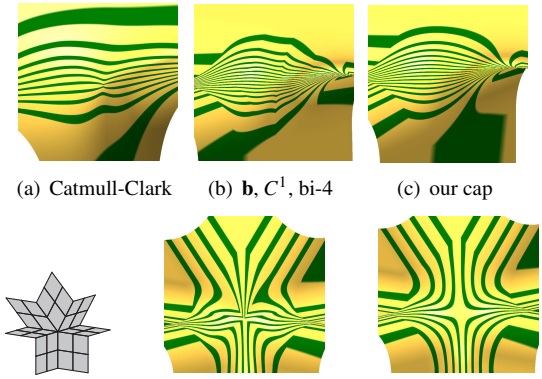

(a) Catmull-Clark (b) $\mathbf{b}, C^1$, bi-4 (c) our cap

(d) input (e) bi-4, no β (f) our cap

Figure 10: The positive effect of **tensor-border reparameterization** β. (a–c) Input for top row is Fig. 7b, a net of valence $n = 6$. The images zoom in on the central point. (a) Catmull-Clark subdivision, for comparison. (b) Bi-4 construction for even valence $n = 6$ using 2×2 patches per sector that match $\mathbf{b}$ without reparameterization. (c) Our bi-4 construction with one patch per sector that matches $\mathbf{b}$ after reparameterization by β. (d) Input CC-net of valence $n = 7$. (e) Bi-4 construction with one patch per sector [29], matching $\mathbf{b}$ directly. (f) Our bi-4 construction with one patch per sector.

Increased smoothness at the central point. We observed that, when enforcing no more than tangent plane continuity at the central point, the highlight line distribution deteriorates with increasing valence n, see Fig. 11b. Our construction achieves a more uniform distribution by enforcing curvature continuity at the central point, see Fig. 11c. The construction carefully relates (distributes), via a symmetric reparameterization σ of degree bi-4 (detailed in Appendix B), the degrees of freedom at the center to n patches meeting at the center as follows. The partial derivatives $\partial_s^i\partial_t^j(\mathbf{a}\circ\sigma)$, $i+j \le 2$ are then computed for a still undetermined quadratic map $\mathbf{a}$ (for this the composition involves only σ_{ij}, $i+j \le 2$). Then the quadratic expansion in terms of the partial derivatives is expressed in the BB-coefficients $\mathbf{p}^k_{ij}, i+j \le 2$ (circles in Fig. 8a) and this satisfies (2). The map $\mathbf{a}$ is determined in the next step.

Choice of Central point and Functionals.
Since the cap is only of degree bi-4, we did not expect $\mathcal{F}_5$ to play a role in determining the *central point*. However, testing the functionals $\mathcal{F}_k$ and $\mathcal{F}^*_k$ on many inputs, e.g. Fig. 7, proved $\mathcal{F}_5$ to consistently yield better highlight line distributions than $\mathcal{F}^*_r$ and functionals $\mathcal{F}_\kappa$ with

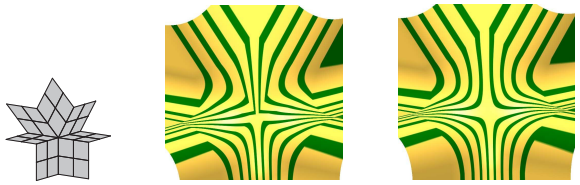

(a) input (b) G^1 at center (c) G^2 at center

Figure 11: The positive effect of **increased smoothness at the central point** on input of CC-net (a).

lower κ (see Fig. 12a-c). The resulting central points were then distilled into the assignment (5) with weight e^{def} that adjusts the average.

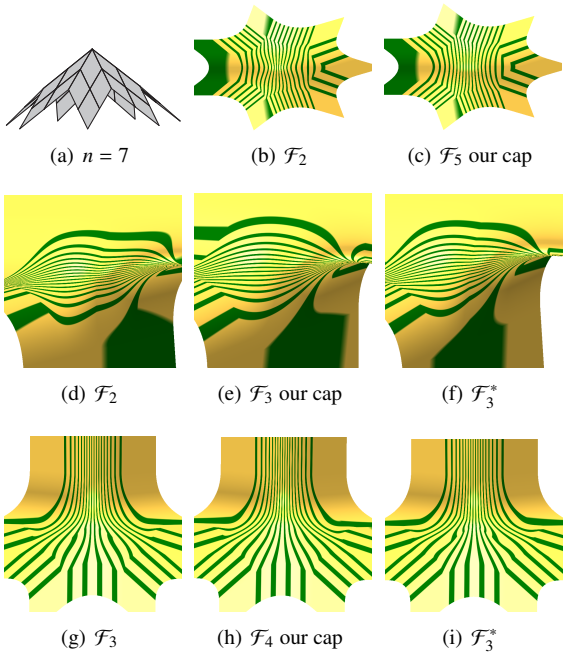

(a) $n = 7$ (b) $\mathcal{F}_2$ (c) $\mathcal{F}_5$ our cap

(d) $\mathcal{F}_2$ (e) $\mathcal{F}_3$ our cap (f) $\mathcal{F}_3^*$

(g) $\mathcal{F}_3$ (h) $\mathcal{F}_4$ our cap (i) $\mathcal{F}_3^*$

Figure 12: **Comparing functionals** for the bi-4 construction. (a–c) Setting the default central point: $\mathcal{F}_5$ is best. The central point is fixed by (5) in (d-i). (d-f) The input is Fig. 7b. $\mathcal{F}_3$ excels. (g-i) The input is Fig. 7d. $\mathcal{F}_4$ excels for higher valence.

Once the central point is fixed in this manner, minimization in terms of the remaining $n+5$ BB-coefficients showed that $\mathcal{F}_3$ should be used for $n = 5, 6, 7$ and $\mathcal{F}_4$ for $n = 8, 9, 10$. This is illustrated in Fig. 12: for lower valencies such as the 6−valent 'beam' (see Fig. 12d-f) $\mathcal{F}_3$ is better than $\mathcal{F}_2$ and $\mathcal{F}_3^*$, while for higher valencies, e.g. for $n > 7$, $\mathcal{F}_4$ yields the best highlight line distribution (see Fig. 12g-i).

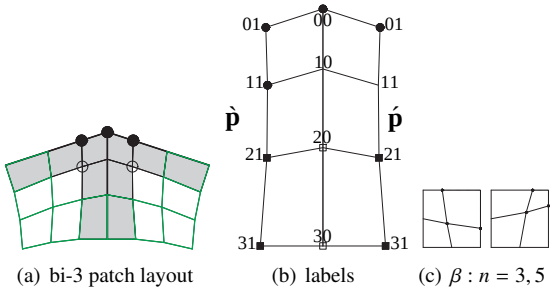

(a) bi-3 patch layout (b) labels (c) $\beta : n = 3, 5$

Figure 13: **Bi-3 construction using one patch per sector.** Layout, notation and tensor-border reparameterization β.

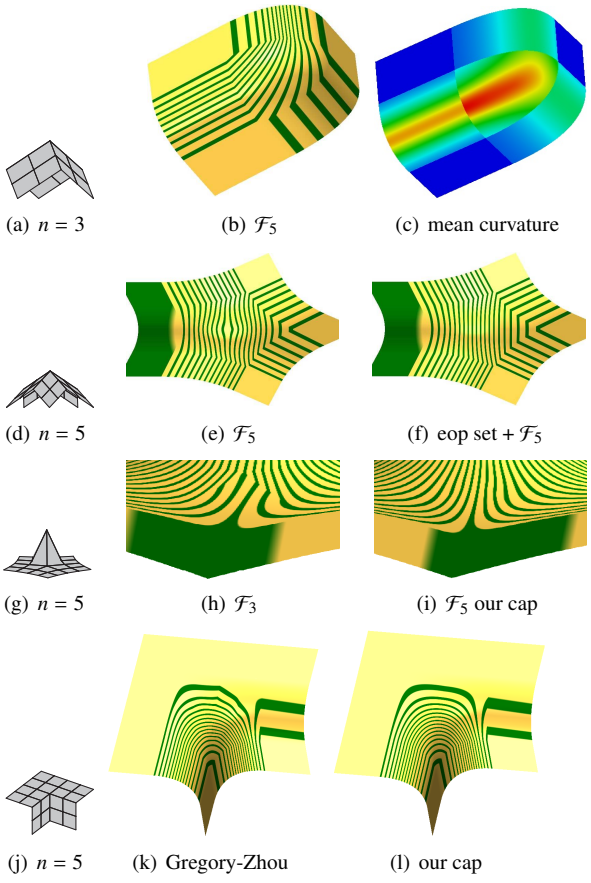

(a) $n = 3$ (b) $\mathcal{F}_5$ (c) mean curvature

(d) $n = 5$ (e) $\mathcal{F}_5$ (f) eop set + $\mathcal{F}_5$

(g) $n = 5$ (h) $\mathcal{F}_3$ (i) $\mathcal{F}_5$ our cap

(j) $n = 5$ (k) Gregory-Zhou (l) our cap

Figure 14: **Bi-3 construction (one patch per sector)** for $n = 3, 5$. Row (a,b,c): Although the cap is only G^1, a jump in the mean curvature (c) is observed only along the tensor-border, not internally. The highlights (b) confirm good quality. (A closeup, comparing the surface to [3], was shown in Fig. 2.) Row (d,e,f): Setting the central point (*eop*) by (5), before minimizing $\mathcal{F}_5$ improves the highlight lines. Row (g,h,i): Also for $n = 5$, the functional $\mathcal{F}_3$ yields poorer highlight lines (h) than our choice $\mathcal{F}_5$ in (i). Our bi-3 n-patch construction (l) has a better highlight line distribution than the bi-3 $2\times2\times n$ cap (k) according to [3].

4.2. ***Caps of degree bi-3 when*** $n \in \{3,5\}$

In the practically important cases $n \in \{3,5\}$, well-shaped bi-3 caps can be constructed as follows. (We conjecture that for $n > 5$ no n-patch constructions of degree bi-3 exist that deliver consistently good highlight line distributions.) With the layout of Fig. 13a,b and reparameterization (1), we obtain

$$\grave{\mathbf{p}}_{20} := \frac{3(\grave{\mathbf{p}}_{21} + \acute{\mathbf{p}}_{21}) - \mathsf{c}(\grave{\mathbf{p}}_{31} + \acute{\mathbf{p}}_{31})}{2(3-\mathsf{c})}, \qquad (2^3)$$

where the tag with the superscript is to remind the reader of the analogous equation of (2) in the bi-4 case. The BB-coefficients $\grave{\mathbf{p}}_{11}$, $\acute{\mathbf{p}}_{11}$ are the unique solution of the $n \times n$ linear (vertex enclosure) system of equations

$$\begin{aligned}&(3-\mathsf{c})\Big(3\mathsf{c}(\grave{\mathbf{p}}_{11} + \acute{\mathbf{p}}_{11}) - (3-2\mathsf{c})\Big((\grave{\mathbf{p}}_{01} + \acute{\mathbf{p}}_{01}) - 2(1-\mathsf{c})\grave{\mathbf{p}}_{00}\Big)\Big)\\ &= -2\mathsf{c}^2\Big(\mathsf{c}(\grave{\mathbf{p}}_{31} + \acute{\mathbf{p}}_{31}) - 3(\grave{\mathbf{p}}_{21} + \acute{\mathbf{p}}_{21})\Big). \qquad (7)\end{aligned}$$

(When n is odd, the system is of full rank.) To achieve consistency of the assignment of $\grave{\mathbf{p}}_{20}$ with the tensor-border, the reparameterization β of the input tensor-border $\mathbf{b}$ is set to

$$a(u) := \frac{1-\mathsf{c}(1-u)}{1-\mathsf{c}}, \quad b(u) := \frac{\mathsf{c}(1-u)u}{1-\mathsf{c}}. \qquad (3^3)$$

Fig. 13c shows β for valencies $n = 3, 5$. For higher valencies, the denominator $(1-\mathsf{c})$ results in increasingly non-uniform parameter lines of β and poorer shape. Since the two boundary layers are pinned down by $\mathbf{b} \circ \beta$, only the central point of the cap and its tangents need to be determined (the bullets in Fig. 13a).

For $n = 3$, the central point and its tangents are obtained by minimizing $\mathcal{F}_5$ over all 3 patches. The resulting bi-3 cap turns out to be G^2 at the center, although not constructed as such. Fig. 14b,c displays a typical result.

For $n = 5$, minimizing $\mathcal{F}_5$ to determine the center point and its tangents yields poor highlight line distribution for convex configurations as illustrated in Fig. 14e. Instead, as for the bi-4 construction, we set the central point (eop) by (5), now with $e^{def} := 0.22$. Only then do we determine the tangent plane by minimizing $\mathcal{F}_5$ over the $n = 5$ patches. This improves the highlight lines to those in Fig. 14f. Comparing Fig. 14h to Fig. 14i makes the argument for choosing $\mathcal{F}_5$ when the degree is bi-3 and $n = 5$. Note that for $n = 5$, the cap is generically not G^2 at the center. Given the low valence, this has no ill effect. In summary, while caps consisting of n bi-3 patches seem unfit for higher valences, the careful approach above results in good highlight lines for the important practical cases $n = 3, 5$.

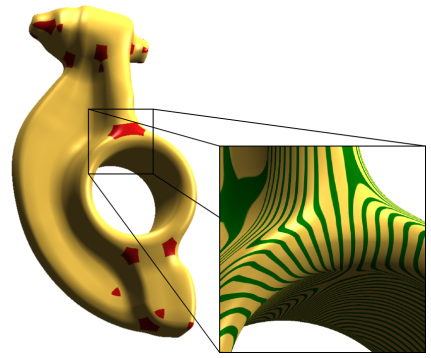

(a) rocker arm

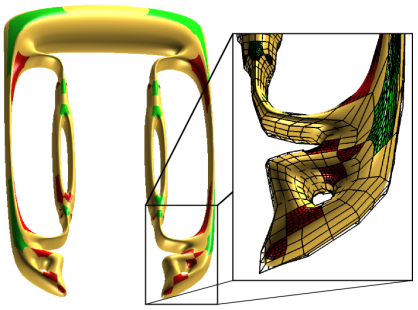

(b) compliant grip

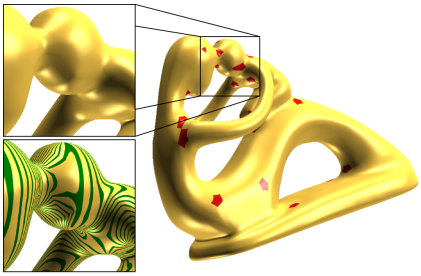

(c) fertility figurine

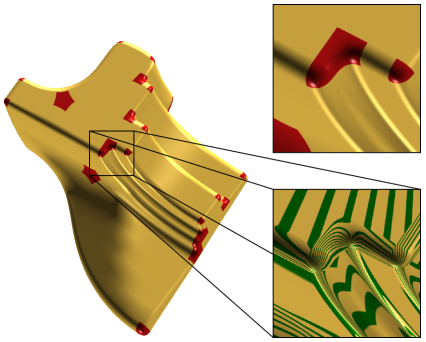

(d) fan disk

Figure 15: **Quad models converted** into CAD-compatible polynomial splines: bi-2 splines (gold), G^1 caps of degree bi-3 = red, bi-4 = green (in b).

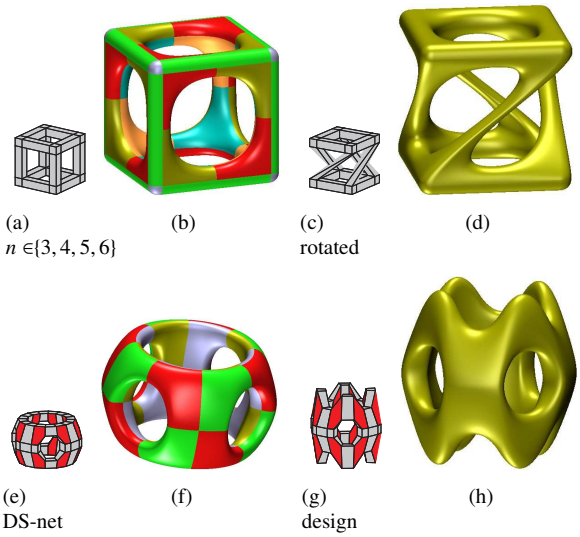

Figure 16: **Combining caps of different degree** using the constructions of Section 4 and Section 4.2 (one polynomial piece per sector): (a,c) CC-net with points of valence $n = 3,4,5,6$. (b,d) 3- and 5-sided caps use bi-3 patches, 6-sided caps use bi-4 patches. In (b) only the green facets are of degree bi-2. (e,g) DS-net with 4- and 5-sided facets. (f,h) The 5-sided caps use bi-3 patches.

5. Modeling with bi-2 splines completed by G^1 caps consisting of n patches of degree bi-3 and bi-4

Fig. 15 illustrates how the caps of Section 4 and Section 4.2 complete the conversion of quad meshes to bi-2 spline control nets with caps. The result is a collection of fully CAD-compatible tensor-product splines. We observe good highlight line distribution also when two caps are directly adjacent, e.g. two pentagonal caps shown in the enlargement of Fig. 15a, and a three-sided cap joining a five-sided cap in Fig. 15d. The examples of Fig. 16b,d are constructed to confirm in detail that caps of different valence work well side-by-side: the models in Fig. 16f,h have no bi-2 patches at all.

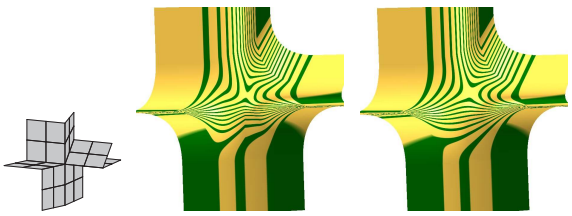

Figure 17: **Comparison** of (b) 2×2 cap of degree bi-3 Appendix C and (c) the bi-4 cap of Section 4.

Fig. 17 shows that while the 2×2 construction of degree bi-3 of Appendix C does remarkably well, our default single-bi-4-patch-per-sector construction of Section 4 handles truly difficult blends more gracefully.

The main role of the DS-net is to unify the treatment of control nets. However, DS-nets with multi-sided facets, appear naturally when blending basic shapes, as was already demonstrated in Fig. 1. In Fig. 18, a DS-net provides one layer of patches (three of one sector are emphasized in yellow in Fig. 18a, top) to transition from the exact rational cylinder to a polynomial tensor-border. A bi-4 cap constructed as in Section 4 (blue in Fig. 18a, top) then smoothly completes the joining of the cylinders.

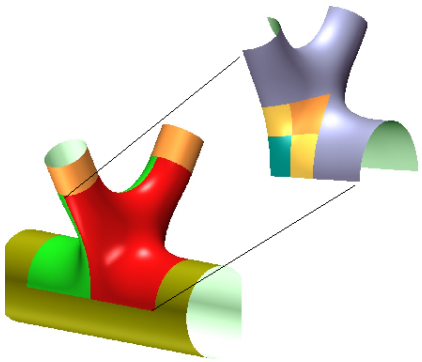

Figure 18: **Joining cylinders** using caps of degree bi-4 and $n = 8$.

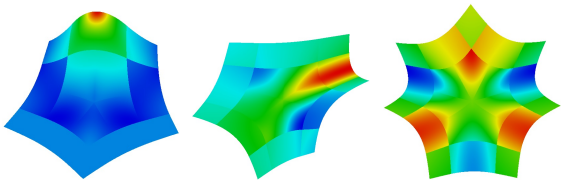

Figure 19: Mean curvature of test surfaces from Fig. 7.

We conclude the gallery of examples with Fig. 19. The mean curvature images of Fig. 19 demonstrate that the changes in curvature between the bi-2 complex and the cap are typically no more pronounced than within the C^1 bi-2 complex itself. The interior of the cap is in fact often smoother, making the cap a natural piece of the bi-2 complex.

6. Conclusion

Bi-quadratic splines with bi-4 caps (bi-3 for $n = 3,5$) often suffice to represent and smoothly blend inner surfaces or mechanical parts and can deliver well-distributed highlight lines. Similar constructions, of

higher degree, can fill-in holes in C^2 bi-3 spline complexes. But while splines of degree bi-3 can model inflections along boundary curves, both hand-crafted and algorithmically-generated quad-meshes model inflections as transitions between (bi-linear) pieces so that the extra flexibility of bi-3 patches is often not needed – while overall lower degree and complexity is appreciated for downstream manipulation and analysis.

This paper provides correspondingly simple yet subtle recipes to complete a collection of bi-2 patches into a smooth surface. The algorithms are based on several carefully chosen reparameterizations of the input data. They improve in particular on the standard C^1 extension that leads to a rapid change in parameterization near the center of the cap.

Early on, experiments yielding poor highlight line distributions dissuaded us from using functionals $\mathcal{F}_k$ or $\mathcal{F}_k^*$ on all free parameters. Only once had good reparameterizations and had increased the smoothness at the central point did we successfully apply functionals. We chose degrees of freedom by comparing their impact on a large number of challenging test cases and this improvement carried over to a broader set of surfaces from quad meshes: The result are surface caps in a CAD-compatible representation of low polynomial degree that naturally complete a C^1 bi-2 spline complex.

Acknowledgements. The work was supported in part by NSF Grant CCF-1117695.

[1] K.-P. Beier, Y. Chen, Highlight-line algorithm for realtime surface-quality assessment, Computer-Aided Design 26 (4) (1994) 268–277, /cise/research/SurfLab/geogp/projects/SGOL, highlight.cpp. doi:http://dx.doi.org/10.1016/0010-4485(94)90073-6.

[2] D. Doo, M. Sabin, Behaviour of recursive division surfaces near extraordinary points, Computer-Aided Design 10 (1978) 356–360.

[3] J. A. Gregory, J. Zhou, Filling polygonal holes with bicubic patches, Computer Aided Geometric Design 11 (4) (1994) 391–410.

[4] C. T. Loop, S. Schaefer, G^2 tensor product splines over extraordinary vertices, Comput. Graph. Forum 27 (5) (2008) 1373–1382.

[5] K. Karčiauskas, J. Peters, Biquintic G^2 surfaces, in: R. J. Cripps, G. Mullineux, M. A. Sabin (Eds.), 14th Itl Conference on Mathematics of Surfaces, 2013, pp. 213–236.

[6] T. Ueshiba, G. Roth, Generating smooth surfaces with bicubic splines over triangular meshes: toward automatic model building from unorganized 3D points, in: 3DIM99, 1999, pp. 302–311.

[7] J. Fan, J. Peters, Smooth bi-3 spline surfaces with fewest knots, Computer Aided Design 43 (2) (2011) 180–187, jCAD 1686.

[8] T. DeRose, Geometric continuity: A parametrization independent measure of continuity for computer aided design, Ph.D. thesis, UC Berkeley, California (1985).

[9] J. Peters, Geometric continuity, in: Handbook of Computer Aided Geometric Design, Elsevier, 2002, pp. 193–229.

[10] R. Barnhill, J. Gregory, Compatible smooth interpolation in triangles, J of Approx. Theory 15 (3) (1975) 214–225.

[11] J. A. Gregory, Smooth interpolation without twist constraints, Academic Press, 1974, pp. 71–88.

[12] D. Plowman, P. Charrot, A practical implementation of vertex blend surfaces using an n-Sided patch, in: G. Mullineux (Ed.), Proceedings of the 6th IMA Conference on the Mathematics of Surfaces (IMA-94), Vol. VI of Mathematics of Surfaces, Clarendon Press, Oxford, 1996, pp. 67–78.

[13] T. DeRose, C. Loop, The S-patch: a new multisided patch scheme, ACM Trans. on Graphics 8 (3) (1989) 204–234.

[14] B. R. Piper, Visually smooth interpolation with triangular Bézier patches, in: G. Farin (Ed.), Geometric Modeling : Algorithms and New Trends, SIAM, Philadelphia, 1987, pp. 221–233.

[15] L. A. Shirman, C. H. Sequin, Local surface interpolation with bezier patches, Computer Aided Geometric Design 4 (4) (1987) 279–295.

[16] J. Peters, C^1-surface splines, SIAM J of Numer. Anal. 32 (2) (1995) 645–666.

[17] J. Wallner, H. Pottmann, Spline orbifolds, in: Curves and surfaces with applications in CAGD (Chamonix–Mont-Blanc, 1996), Vanderbilt Univ. Press, Nashville, TN, 1997, pp. 445–464.

[18] X. Gu, Y. H. 0001, H. Qin, Manifold splines, Graphical Models 68 (3) (2006) 237–254. doi:http://dx.doi.org/10.1016/j.gmod.2006.03.004.

[19] R. Pfeifle, H.-P. Seidel, Faster evaluation of quadratic bivariate DMS spline surfaces, in: W. A. Davis, B. Joe (Eds.), Proceedings of Graphics Interface '94, Banff, Alberta, Canada, Canadian Information Processing Society, Morgan Kaufmann, 1994, pp. 182–189. doi:http://visinfo.zib.de/EVlib/Show?EVL-1994-12.

[20] E. Catmull, J. Clark, Recursively generated B-spline surfaces on arbitrary topological meshes, Computer-Aided Design 10 (1978) 350–355.

[21] K. Karciauskas, J. Peters, U. Reif, Shape characterization of subdivision surfaces – case studies, Computer Aided Geometric Design 21 (6) (2004) 601–614.

[22] U. Reif, Biquadratic G-spline surfaces, Computer Aided Geometric Design 12 (2) (1995) 193–205.

[23] J. Peters, Smooth mesh interpolation with cubic patches, Computer Aided Design 22 (2) (1990) 109–120.

[24] M. Halstead, M. Kass, T. DeRose, Efficient, fair interpolation using Catmull-Clark surfaces, in: Proc 20th Annual Conference on Computer Graphics and Interactive Techniques, SIGGRAPH '93, ACM, New York, NY, USA, 1993, pp. 35–44. doi:10.1145/166117.166121.

[25] G. Greiner, Variational design and fairing of spline surfaces, Computer Graphics Forum 13 (3) (1994) 143–154.

[26] G. Greiner, Curvature approximation with application to surface modeling, in: J. Hoschek, P. Kaklis (Eds.), Advanced Course on FAIRSHAPE, B. G. Teubner, 1996.

[27] J. Loos, G. Greiner, H.-P. Seidel, Modeling of surfaces with fair reflection line pattern, in: B. Werner (Ed.), Proceedings of the International Conference on Shape Modeling and Applications (SMI-99), IEEE Computer Society, Los Alamitos, CA, 1999, pp. 256–263.

[28] R. F. Sarraga, A variational method to model G1 surfaces over triangular meshes of arbitrary topology in R3, ACM Trans. Graph 19 (4) (2000) 279–301.

[29] G. Westgaard, H. Nowacki, Construction of fair surfaces over irregular meshes, in: Symposium on Solid Modeling and Applications, 2001, pp. 88–98.

[30] J. Peters, Smooth free-form surfaces over irregular meshes generalizing quadratic splines, Computer Aided Geometric Design

10 (1993) 347–361.

Appendix A: The generating functions for a CC-net cap

To express the solution in terms of CC-net points as labeled in Fig. 6a, we re-use the pre-computed table of $h_{ij}^{k,m}$ for the DS-net Fig. 6b, but combine the entries as follows:

$$\mathbf{p}_{ij}^{s} := \sum_{k=0}^{n-1}\sum_{m=1}^{2} \bar{h}_{ij}^{k,m}\mathbf{q}_{m}^{s-k} + \bar{h}_{ij}^{E}E, \qquad (6')$$

$$\bar{h}_{ij}^{k,1} := \frac{9}{16}(h_{ij}^{k,4} + h_{ij}^{k-1,2}) + \frac{3}{16}(h_{ij}^{k,1} + h_{ij}^{k-1,1} + h_{ij}^{k,3} + h_{ij}^{k-1,3}) + \frac{1}{16}(h_{ij}^{k,2} + h_{ij}^{k-1,4});$$

$$\bar{h}_{ij}^{k,2} := \frac{9}{16}h_{ij}^{k,3} + \frac{3}{16}(h_{ij}^{k,2} + h_{ij}^{k,4}) + \frac{1}{16}h_{ij}^{k,1};$$

$$\bar{h}_{ij}^{E} := \frac{9}{16}\sum_{k=0}^{n-1} h_{ij}^{k,1} + \frac{3}{16}\sum_{k=0}^{n-1}(h_{ij}^{k,2} + h_{ij}^{k,4}) + \frac{1}{16}\sum_{k=0}^{n-1} h_{ij}^{k,3}.$$

Appendix B: Central parameterization σ

We construct $\sigma : [0..1]^{2\times n} \to \mathbb{R}^2$ of degree bi-4, along the same principles as the cap of Section 4. Inspired by the good iso-line distribution of the conformal map $z^{4/n}$, $z \in \mathbb{C}$, we use as input a 1-layer CC-net, shown as the red quads in Fig. 6a. The CC-net consists of n copies, rotated by multiples of $\alpha := 2\pi/n$, of the quad with vertices

$$E := \begin{bmatrix}0\\0\end{bmatrix},\ \mathbf{q}_1^0 := \tau\begin{bmatrix}1\\0\end{bmatrix},\ \mathbf{q}_1^1 := \tau\begin{bmatrix}\cos\alpha\\ \sin\alpha\end{bmatrix},\ \alpha := \frac{2\pi}{n},$$

$$\mathbf{q}_2^1 := \frac{n}{2n-4}\frac{\mathbf{q}_1^0 + \mathbf{q}_1^1}{2} \approx (1+i)^{4/n}.$$

The scaling parameter τ is chosen to normalize σ so that $\sigma_{40} = 1$ (see Fig. 20 for the subscripts).

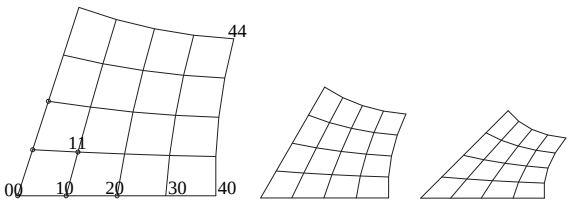

(a) $n = 5$ (b) $n = 6$ (c) $n = 8$

Figure 20: The parameterization σ.

Two parameters of the border reparameterization β are free to choose in (3): any choice of a_2 and b_2 yields

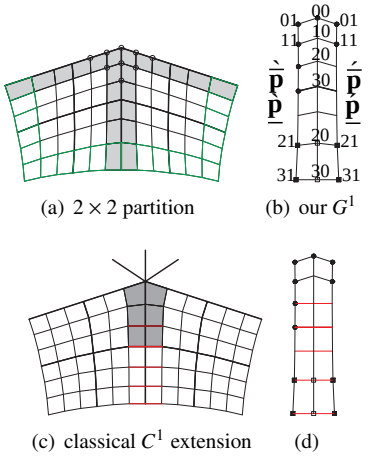

(a) 2×2 partition (b) our G^1

(c) classical C^1 extension (d)

Figure 21: The **2×2 bi-3 construction**. (a,b) our construction. The bottom-most layer of BB-coefficients satisfy G^1 constraints (1). (c,d) C^1 constraints used e.g. in [3]. The C^1 constraints lead to poorer highlight line distributions despite an equal number and distribution of degrees of freedom.

a cap matching the tensor-border. Numerous experiments, as well as consistency with the case $n = 4$ when β is the identity, recommend the choice $b_2^{def} := 0$ and setting a_2^{def} to enforce the internal scaling $\sigma_{30} \approx \frac{3}{4}\sigma_{40}$ (see Fig. 20a).

Symmetry between sectors, flip-symmetry of each sector about its diagonal and smoothness then imply

$$\sigma_{00} := (0,0),\ \sigma_{10} := (d_1, 0),\ \sigma_{11} := (d_2\cos\frac{\alpha}{2}, d_2\sin\frac{\alpha}{2})$$

$$\sigma_{20} := \Big((1 - \frac{4}{3\cos\alpha})d_1 + \frac{4\cos\frac{\alpha}{2}}{3\cos\alpha}d_2, 0\Big).$$

A third scalar parameter, d_3, is available when setting σ_{21} according to symmetry and (2). Symmetry defines the remaining BB-coefficients of σ in terms of d_1, d_2, d_3. The parameters d_1, d_2, d_3 are set to minimize $\mathcal{F}_\kappa(\sigma)$ applied and summed for the two coordinates x and y of one sector. The choices $\kappa = 2, 3, 4, 5$, as well as minimizing $\mathcal{F}_3^*$ all yield very similar results suggesting the formulas:

$$d_1^{def} := \frac{0.24n - 0.75}{n - 3.16}, \quad d_2^{def} := \frac{0.44n - 0.75}{n - 4 + 2.02\sqrt{2}}.$$

Fig. 20 shows the resulting map for $n = 5, 6, 8$.

Appendix C: Bi-3 2×2 split macro-patch caps

For completeness, we provide a third cap construction. Where it is important to keep the polynomial degree to bi-3 also when $n > 5$, G^1 caps can be constructed

from 2×2 split C^1 macro-patches as shown in Fig. 21a. Our construction, see Fig. 21a,b, uses a G^1 transition to the tensor-border $\mathbf{b}$, while constructions such as [3], see Fig. 21c,d, connect C^1 to the tensor-border data. The latter results in poorer highlight line distributions, the more so the higher the valence n. G^1 continuity across the n sector boundaries is assured between adjacent sector sub-patches $\grave{\underline{\mathbf{p}}}$ and $\acute{\underline{\mathbf{p}}}$ including the center point by enforcing $(\overline{1})$ and between sub-patches $\grave{\underline{\mathbf{p}}}$ and $\acute{\underline{\mathbf{p}}}$ attached to $\mathbf{b}$ by $(\underline{1})$:

$$\acute{\overline{\mathbf{p}}}_v + \grave{\overline{\mathbf{p}}}_v = (2\mathsf{c}(1-u)+\gamma u)\grave{\overline{\mathbf{p}}}_u, \quad \mathsf{c} := \cos\frac{2\pi}{n}, \qquad (\overline{1})$$

$$\acute{\underline{\mathbf{p}}}_v + \grave{\underline{\mathbf{p}}}_v = \gamma(1-u)\grave{\overline{\mathbf{p}}}_u, \quad \gamma^{def} := \frac{n-2.3}{2n-7.72}. \qquad (\underline{1})$$

BB-coefficients unconstrained after enforcing the G^1 constraints are marked as the black disks in Fig. 21b. The coefficient

$$\grave{\underline{\mathbf{p}}}_{20} := \frac{6(\grave{\underline{\mathbf{p}}}_{21}+\acute{\underline{\mathbf{p}}}_{21}) - \gamma\mathsf{c}(\grave{\underline{\mathbf{p}}}_{31}+\acute{\underline{\mathbf{p}}}_{31})}{2(6-\gamma\mathsf{c})} \qquad (\underline{2})$$

is made consistent with the input tensor-border $\mathbf{b}$ by a reparameterization β with

$$a(u) := \frac{1-\gamma\mathsf{c}(1-u)}{1-\gamma\mathsf{c}}, \quad b(u) := \frac{\gamma\mathsf{c}(1-u)u}{1-\gamma\mathsf{c}}. \qquad (3^{2\times2})$$

This reparameterization generalizes (3^3) where $\gamma := 1$. The choice of γ^{def} prevents the high distortion of the reparameterization (cf. Fig. 22a vs. Fig. 22b) that limited the applicability of the single-patch bi-3 construction of Section 4.2. The 2×2 split of the patch removes the need for solving (7), the vertex enclosure problem for even valences. More precisely, we can assign

$$\grave{\overline{\mathbf{p}}}_{20} := \frac{6+(\gamma-10)\mathsf{c}+4\mathsf{c}^2}{4\mathsf{c}^2}\grave{\overline{\mathbf{p}}}_{00} + \frac{3}{4\mathsf{c}}(\grave{\overline{\mathbf{p}}}_{11}+\acute{\overline{\mathbf{p}}}_{11}) - \frac{6+(\gamma-4)\mathsf{c}}{8\mathsf{c}^2}(\grave{\overline{\mathbf{p}}}_{01}+\acute{\overline{\mathbf{p}}}_{01}). \qquad (\overline{2})$$

An analogous assignment is impossible in the case of a non-split bi-3 cap since there $\grave{\underline{\mathbf{p}}}_{20}$ is defined by the tensor-border $\mathbf{b}$ via (2^3).

The layout of the BB-coefficients in Fig. 21 is remarkably undistorted also for higher n. The outer, green points (BB-coefficients) match the reparameterized split tensor-border data $\mathbf{b}\circ\beta$, the gray underlaid strips the G^1 conditions between sectors, and the circled points are set by the σ-parametrized quadratic at the central point. As in Section 4, we obtain the symmetric 2×2 bi-3 map σ (see Fig. 22c) by minimizing a functional (here $\mathcal{F}_3$ turned out to be best) over all four subpatches of a sector.

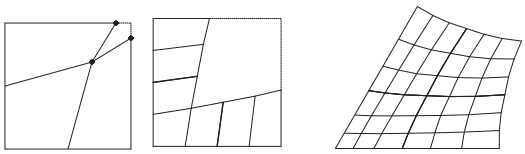

(a) β of Section 4.2, $n=6$ (b) β: 2×2 split (c) 2×2 split σ

Figure 22: Tensor-border **reparameterization** β of the 2×2 bi-3 macro patch construction: (a) before and (b) after split. (c) Bi-3 parameterization σ.

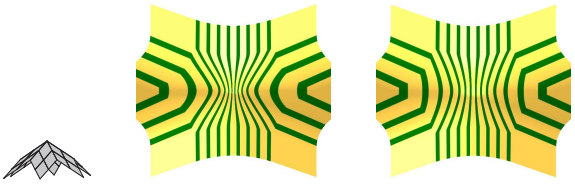

(a) $n=6$ (b) $\mathcal{F}_3$ (c) eop set + $\mathcal{F}_3$

Figure 23: Explicitly setting the **central point** (eop) is beneficial also for the **2×2 bi-3** macro patch construction.

As in Section 4, determining the unknowns of the cap directly by minimizing $\mathcal{F}_3$ over all $4n$ sub-patches of the cap yields pinched highlight lines for convex input data (see Fig. 23b). However, if we first fix the central point by (5), now with $e^{def} := \frac{0.02n+1.5}{n+1.75}$, and then minimize $\mathcal{F}_3$ to set the remaining coefficients, the result is good, as illustrated in Fig. 23c.